Oxidative Metabolism of Combretastatin A-1 Produces Quinone Intermediates with the Potential To Bind to Nucleophiles and To Enhance Oxidative Stress via Free Radicals

ARTICLE *in* CHEMICAL RESEARCH IN TOXICOLOGY · JANUARY 2008

Impact Factor: 3.53 · DOI: 10.1021/tx7002195 · Source: PubMed

5 AUTHORS, INCLUDING:

Martin Christlieb
University of Oxford
41 PUBLICATIONS **568** CITATIONS
SEE PROFILE

Edyta Madej
Ruhr-Universität Bochum
17 PUBLICATIONS **205** CITATIONS
SEE PROFILE

Michael R L Stratford
University of Oxford
192 PUBLICATIONS **4,634** CITATIONS
SEE PROFILE

Oxidative Metabolism of Combretastatin A-1 Produces Quinone Intermediates with the Potential To Bind to Nucleophiles and To Enhance Oxidative Stress via Free Radicals

Lisa K. Folkes,* Martin Christlieb, Edyta Madej, Michael R. L. Stratford, and Peter Wardman

University of Oxford, Gray Cancer Institute, P.O. Box 100, Mount Vernon Hospital, Northwood, Middlesex HA6 2JR, United Kingdom

Received June 20, 2007

Combretastatins are stilbene-based, tubulin depolymerization agents with selective activity against the tumor vasculature; two variants (A-1 and A-4) are currently undergoing clinical trials. Combretastatin A-1 (CA1) has a greater antitumor effect than combretastatin A-4 (CA4). We hypothesized that this reflects the enhanced reactivity conferred by the second (*ortho*) phenolic moiety in CA1. Oxidation of CA1 by peroxidase, tyrosinase, or Fe(III) generates a species with mass characteristics of the corresponding *ortho*-quinone Q1. After administration of CA1-*bis*(phosphate) to mice, the hydroquinone–thioether conjugate $Q1H_2$-SG, formed from the nucleophilic addition of GSH to Q1, was detected in liver. In competition, electrocyclic ring closure of Q1, over a few minutes at pH 7.4, leads to a second *ortho*-quinone product Q2, characterized by exact mass and NMR. This product was also generated by human promyelocytic leukemia (HL-60) cells in vitro, provided that superoxide dismutase was added. Q2 is highly reactive toward glutathione (GSH) and ascorbate, stimulating oxygen consumption in a catalytic manner. Free radical intermediates formed during autoxidation of CA1 were characterized by EPR, and the effects of GSH and ascorbate on the signals were studied. Pulse radiolysis was used to initiate selective one-electron oxidation or reduction and provided further evidence, from the differing absorption spectra of the radicals formed on oxidation of CA1 or reduction of Q2, that two different quinones were formed on oxidation of CA1. The results demonstrate fundamental differences between the pharmacological properties of CA1 and CA4 that provide two possible explanations for their differential activities in vivo: oxidative activation to a quinone intermediate likely to bind to protein thiols and possibly to nucleic acids and stimulation of oxidative stress by enhancing superoxide/hydrogen peroxide production. The observation of the GSH conjugate $Q1H_2$-SG in vivo provides a new marker for oxidative metabolism of relevance to current clinical trials of CA1-*bis*(phosphate) (OXi4503).

Introduction

Targeting the tumor vasculature is a therapeutic strategy attracting increasing attention in cancer therapy (*1–4*). One class of vascular-targeting agents, the combretastatins (*5*), are tubulin-depolymerizing drugs that selectively attack the tumor vasculature (*6–8*). Clinical trials of phosphate ester prodrugs of two examples are in progress: combretastatins A-4 (CA4)[1] and A-1 (CA1; OXi4500); see Scheme 1 (e.g., see refs *9–11*; Cancer Research UK Trial Protocol No. PH1/098). The *bis*(phosphate) prodrug of CA1 (CA1P; OXi4503) showed more potent antivascular and antitumor effects than the phosphate prodrug of CA4 when administered as a single agent to a variety of murine tumors (*12–14*). However, the mechanisms responsible for these differences are unclear. It was suggested that OXi4503 might have an additional cytotoxic mechanism (*1*), although previous comparative in vitro studies with CA1 and CA4 focused on overcoming resistance to anthracyclines (*15*).

We hypothesized that the additional hydroxy substituent in CA1 as compared to CA4 potentially offered a greater susceptibility to oxidative metabolism and the formation of free radicals. Thus, other *ortho*-dihydroxybenzenes (catechols) are easily oxidized to *ortho*-quinones, reactive toward thiols and other biological nucleophiles and forming free radicals (*16*). In this study, we have explored in experimental models the potential for CA1 to bind to cellular nucleophiles or to increase oxidative stress through radical formation via a quinone formed on oxidation of CA1. In the event, our studies revealed two quinone intermediates, which we abbreviated to Q1 and Q2 (see Scheme 1). These could both be prepared chemically by oxidation of CA1, by varying the oxidation conditions as described below. The reactivity of quinone intermediates toward glutathione (GSH, Scheme 1), observed in chemical models, was confirmed following administration of CA1P to mice. Evidence for free radical formation, and oxygen consumption, on the interaction of the quinones with GSH or ascorbate ($AscH^-$) demonstrated further reactions following oxidative metabolism of CA1; these have potential importance in the mode of action, or the toxicology, of this compound. Comparisons of oxidation rates in enzyme-catalyzed reactions of CA1 and CA4 were made to identify differences between the two combretastatins, and the redox properties of the drugs and their free

* To whom correspondence should be addressed. Tel: +44 1923 828 611. Fax: +44 1923 835 210. E-mail: folkes@gci.ac.uk.

[1] Abbreviations: $AscH^-$, ascorbate; CA1, combretastatin A-1; CA1P, combretastatin *bis*(phosphate); CA4, combretastatin A-4; DMPO, 5,5-dimethyl-1-pyrolline-*N*-oxide; HRP, horseradish peroxidase; DTPA, diethylenetriaminepentaacetic acid; Q1, combretastatin A-1 quinone; $Q1H_2$-SG, glutathione thioether conjugate of combretastatin A-1; Q2, quinone formed on ring closure of Q1; SOD, superoxide dismutase; TFA, trifluoroacetic acid.

10.1021/tx7002195 CCC: $37.00
Published on Web 10/18/2007

Scheme 1. Structures of Combretastatins A-1 (CA1) and A-4 (CA4) and the Reaction Pathways Following Oxidation of CA1 Discussed in the Text

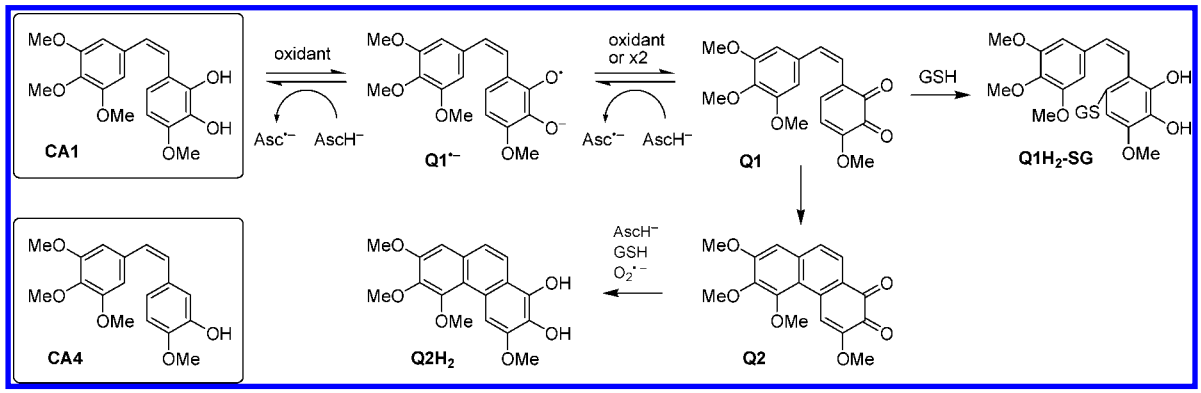

radical oxidation products were explored to help understand reaction mechanisms.

Materials and Methods

Materials. CA1, CA1P, and CA4 were obtained from Oxigene Inc.; solutions were freshly prepared each day and protected from light. PBS (0.14 M NaCl, 3 mM KCl, and 10 mM phosphate) was from Oxoid Ltd. (Basingstoke, Hampshire, United Kingdom). HRP type VIA, tyrosinase from mushroom, SOD from bovine erythrocytes, and all other chemicals were obtained from Sigma (Poole, United Kingdom).

Oxidation of CA1 to Q1. CA1 was dissolved in ethanol, and water was added to give a final concentration of 0.8 mM in 1% ethanol; this was mixed with an equal volume of $FeCl_3$ (4 mM) in H_2SO_4 (1 mM). After 1 min, to prevent further oxidation to Q2, $FeCl_3$ was removed by solid phase extraction. The column (Discovery C18, 100 mg, 1 mL) (Supelco, Poole, United Kingdom) was preconditioned with methanol followed by water, the sample was loaded, and the iron was removed by washing with water followed by 20% methanol. The quinone (containing ~50% unchanged CA1) was eluted with acetonitrile. The identity was confirmed by LC/MS and UV/vis absorbance. The mixture of quinone and CA1 was stored in acetonitrile solution and, in the dark in the absence of water, was stable throughout the day.

Oxidation of CA1 to Q2. CA1 was dissolved in ethanol; then, water was added to give a 2 mM solution containing 4% v/v ethanol, it was mixed with an equal volume of $FeCl_3$ (8 mM) in H_2SO_4 (2 mM), and the mixture was stirred for 45 min before extracting it in ethyl acetate. The product was preabsorbed onto silica and purified through a silica column eluting with 3:1 hexane:ethyl acetate. The red fractions were collected and dried down on a rotary evaporator. The purity and identity were checked by HPLC comparing them to previously recorded spectra with detection at 265 nm.

Oxidation of CA1 or CA4 by H_2O_2/Horseradish Peroxidase (HRP). Reaction rates of CA1 and CA4 with HRP compound I were measured by stopped-flow spectrophotometry as previously described (*17*). CA1 and CA4 were dissolved in ethanol and diluted with water to give a stock solution containing 4% v/v ethanol. Further dilution in phosphate buffer solution (10 mM, pH 7 or 7.4) gave a maximum ethanol concentration of 0.1% v/v. HRP compound I was formed by premixing (1 s) equimolar HRP and H_2O_2 (0.43 μM), and the reaction was monitored after adding CA1 or CA4 (0.1–2.5 μM) using double-mix conditions at 25 °C. The formation of HRP compound II was monitored at 411 nm; five experiments were averaged and fitted to first-order (exponential) kinetics at five different concentrations of CA1 or CA4. Second-order rate constants were calculated from the linear fit of a plot of first-order rate constants against concentration.

Oxidation of CA1 or CA4 by Tyrosinase or Lactoperoxidase. Solutions of CA1 or CA4 (100 μM) were treated with mushroom tyrosinase (7.5 μg/mL, activity 2590 U/mg) at 37 °C in PBS or with bovine erythrocyte lactoperoxidase (10 μg/mL, activity 5100 U/mg) and H_2O_2 (1 mM) at 28 °C in 25 mM phosphate buffer solution containing DTPA (100 μM). Reactions were monitored by HPLC.

Oxidation of CA1 by HL60 Cells. Human pro-myelocytic leukemia cells (HL-60) (European Collection of Cell Cultures, Salisbury, United Kingdom) were maintained in RPMI medium with 10% fetal calf serum, 2 mM L-glutamine, 100 units/mL penicillin, and 100 μg/mL streptomycin. CA1 (87 μM) in PBS containing diethylenetriaminepentaacetic acid (DTPA, 100 μM) was mixed with HL-60 cells (2×10^5) with or without the addition of SOD (125 μg/mL) at 37 °C. The loss of CA1 and formation of Q2 was measured by HPLC.

HPLC/MS, NMR, and Mass Spectrometry of CA1, Q1, and Q2. HPLC was carried out using a gradient of 10 mM ammonium formate containing 20% methanol (A) and methanol (B), 30–100% B over 3 min at 1 mL/min. A Hichrom RPB column (100 mm × 3.2 mm) was used with detection by UV–visible absorbance (Waters 2996 diode array detector) and, after diverting 0.8 mL/min to waste, by electrospray mass spectrometry (Waters Micromass ZQ) operating in ES+ mode at 2.5 kV with a cone voltage of 20–22 V. Q2 was chromatographed on an ACE C18 column (125 mm × 3 mm) using a gradient of 10 mM ammonium formate (A) and acetonitrile (B), 30–60% (B) over 5 min at 1 mL/min. NMR spectra were recorded on a Varian Mercury VX300 spectrometer (^{1}H NMR at 500 MHz and ^{13}C{^{1}H} NMR at 125.8 MHz) using the residual solvent signal as an internal reference. Mass spectra to measure accurate mass of Q2 were recorded on a Micromass LCT time-of-flight mass spectrometer using positive ion electrospray (ES+) in Z-spray configuration with a capillary voltage of 3.0 kV and a cone voltage of 30 V; accurate mass was assessed to four decimal places using tetraoctylammonium bromide (466.5352 Da) as an internal reference.

Pharmacokinetics and Metabolism of CA1P/CA1 in Mice. CA1P in water (5 mg/mL) was injected IP into CBA female mice with a subcutaneous dorsal CaNT tumor. After 15 min to 2 h, duplicate mice were sacrificed and blood and tissues were removed. Blood was collected into tubes containing 1 mg of K_3EDTA and 1 mg of ascorbic acid and centrifuged (14000*g*, 2 min), and the plasma was stored at −20 °C. Liver, tumor, and kidney samples were removed and homogenized in 4 vol of 2 mg/mL Na_2EDTA/1 mg/mL ascorbic acid and stored at −20 °C before analysis. For CA1 analysis, an aliquot of plasma or homogenate was extracted with an equal volume of ~3 mg/mL desferrioxamine mesylate suspended in acetonitrile, and the supernatant was injected directly into the HPLC. Samples were chromatographed on a Hichrom RPB column (100 mm × 3.2 mm) eluted isocratically with 38% acetonitrile, 75 mM $HClO_4$, and 5 mM KH_2PO_4, pH 2.65, at 0.6 mL/min with a column temperature of 35 °C. A Coulochem 5100A electrochemical detector with a porous graphite electrode was used, operating at +0.35V. To confirm $Q1H_2$-SG formation in vivo, nontumor-bearing SCID male mice were treated as described above along with a nontreated control and sacrificed after 18 min. Tissue homogenates

were extracted with equal volumes of acetonitrile and centrifuged, and the supernatant was dried down under N_2. Samples were reconstituted in 80 μL of 20% methanol in 10 mM sodium formate and chromatographed on a Hichrom RPB column (100 mm × 3.2 mm) with a gradient of 20% methanol in 10 mM ammonium formate changing to 100% methanol, in 5 min at 1 mL/min. Detection using mass spectrometry in ES+ single ion mode (*m/z* 638) was used (cone voltage, 15 V) with samples compared to prepared $Q1H_2$-SG.

Measurement of Oxygen Consumption by Q2 with Antioxidants. Q2 was dissolved in acetonitrile, and phosphate buffer (25 mM, pH 7.43) containing DTPA (100 μM) was added to give a 50 μM solution in 1% v/v acetonitrile; a 3 mL sample was added to a stirred Clark type oxygen electrode chamber without headspace (Rank Brothers, Cambridge, United Kingdom) at 37 °C. Ascorbate (50 μL, 18 mM) or glutathione (100 μL, 90 mM) was added when the signal stabilized to give final concentrations of ~0.3 and 3 mM, respectively, and oxygen consumption was recorded.

Measurement of Oxygen Consumption by CA1/HRP/H_2O_2 with Ascorbate. CA1 (100 μM) and H_2O_2 (10 μM) (3 mL) in the oxygen electrode chamber at 37 °C were mixed with HRP (6.7 μg/mL) for 0, 1, 3, or 10 min before the addition of ascorbate (1 mM final concentration), and oxygen consumption was recorded.

EPR Spectroscopy. A Bruker EMX spectrometer (Bruker, Coventry, United Kingdom) equipped with a high sensitivity cylindrical cavity was used with 100 kHz modulation frequency. Typical spectrometer settings were as follows: modulation amplitude, 0.025 mT (0.1 mT for DMPO experiments); microwave power, 20 mW; sweep rate, 0.024 mT/s (0.2 mT/s for DMPO experiments); time constant, 20 ms (10 ms for DMPO); and gain, 2–4 × 10^5 (4–20 sweeps averaged). Buffers were treated with Chelex 100 resin.

Pulse Radiolysis. The apparatus for irradiating solutions with ~0.5 μs pulses of ~6 MeV electrons and monitoring reactions by kinetic spectrophotometry with submicrosecond resolution has been described (*18*). The interaction of the hydroquinone with azide radicals was measured by pulse radiolysis (6 Gy) of solutions containing CA1 (38 μM) with sodium azide (50 mM) in sodium phosphate buffer (10 mM) at pH 7.35, saturated with either N_2O or N_2O/O_2 80/20 v/v. Radical spectra were measured by calculating the radical extinction coefficient of CA1 or CA4 (50 μM containing 0.05% v/v DMSO) with sodium azide (0.1 M) (4.5 Gy/pulse) at varying wavelengths (240–650 nm). Reduction of Q2 by $O_2^{\bullet-}$ or $CO_2^{\bullet-}$ was studied by dissolving Q2 in acetonitrile and diluting with sodium formate (0.1 M) in sodium phosphate buffer (25 mM, pH 7.4) to give a solution of Q2 (30 μM) in 1% (v/v) acetonitrile/H_2O. Solutions were saturated with O_2 or N_2 before radiolysis (3 Gy/pulse), and the semiquinone spectrum was recorded after 200 μs.

Cyclic Voltammetry. Voltammograms were recorded with an Autolab PGSTAT 20 potentiostat with GPES software (Windsor Scientific, Slough, United Kingdom). The three-electrode system consisted of a working disk (3 mm) glassy carbon electrode (GC), a reference-saturated calomel electrode (SCE), and a platinum wire auxiliary electrode. The reference electrode potential was checked against chemical standard grade potassium hexachloroiridate (IV) (K_2IrCl_6). Before a scan, the working electrode was polished with alumina slurry (0.05 μm) and rinsed with water. CA1 or CA4 was dissolved in DMSO or Q2 in acetonitrile and diluted to provide solutions containing CA1 (0.5 mM) or CA4/Q2 (0.1 mM), supporting electrolyte (KCl) (0.1 M), and phosphate buffer (5–25 mM). Solutions contained 0.5–10% v/v DMSO/H_2O (CA1 or CA4) or 1–10% v/v acetonitrile/H_2O (Q2). To vary the pH, small amounts of concentrated $HClO_4$ or NaOH were added to the working solution. The solutions were bubbled with N_2, and the sweep rate was 0.1 V/s (CA1), up to 9 V/s (CA4), or 0.1–1 V/s (Q2). All experiments were carried out at room temperature (24 ± 2 °C).

Results

Identification of Quinones Produced on Oxidation of CA1. CA1 (λ_{max} 300 nm, Figure 1, mass ~332.1 Da) was initially oxidized by $FeCl_3$ (1 min of oxidation with immediate removal of $FeCl_3$, with only ~50% loss of CA1; see the Materials and Methods) to yield a compound with λ_{max} 282 and 415 nm and mass ~330.1 Da (Figure 1). This is consistent with oxidation of the catechol to the corresponding quinone Q1 (Scheme 1; $C_{18}H_{18}O_6$ = 330.11). The same product, with identical absorption maxima, HPLC retention time, and mass spectral pattern, was also initially produced on oxidation of CA1 by HRP compound I (see below), lactoperoxidase, tyrosinase, or HL60 cells (in the presence of SOD) (data not shown).

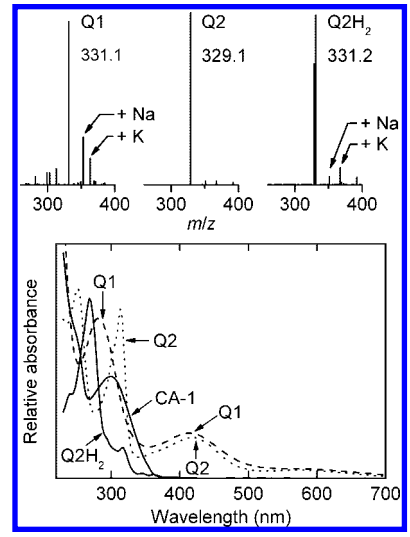

Figure 1. UV/vis spectrum of CA1 (—), Q1 (---), Q2 (▪▪▪), and $Q2H_2$ (—) and corresponding mass spectra measured by LC/MS, masses of labeled peaks corresponding to the protonated molecular ions. Absorbances have been arbitrarily scaled for convenient graphical presentation as extinction coefficients are not available for all species.

Q1 was unstable in aqueous solution, resulting in the formation of a more hydrophobic product absorbing at 312 and 420 nm and with mass of ~328.1 Da (Figure 1), consistent with the formation of a product Q2 resulting from electrocyclic ring closure (Scheme 1). Under the same HPLC conditions, no similarly retained products were formed on oxidation of CA4.

To support the identity of Q2, it was synthesized by oxidation of CA1 with $FeCl_3/H_2SO_4$ and analyzed by accurate mass measurement and ^1H and ^{13}C NMR. *m/z* (ES^+): 329.1 (MH^+, 100%) and 679.2 (40%). Calculated $C_{18}H_{17}O_6$ (MH^+), 329.1025; observed, 329.1038. ^1H NMR ($CDCl_3$,D_2O,500 MHz): δ_H 8.43 (1H, s, ArCH), 7.91 (1H, d, J = 8.5 Hz, ArCH), 7.55 (1H, d, J = 8.5 Hz, ArCH), 6.91 (1H, s, ArCH), 4.02 (3H, s, OMe), 3.99 (3H, s, OMe), 3.95 (3H, s, OMe), and 3.91 (3H, s, OMe). ^{13}C NMR ($CDCl_3$): δ_C 178.9 (C═O), 176.3 (C═O), 155.4, 151.7, 151.1, 144.2, 136.6, 133.4, 127.3, 125.6, 124.9, 120.0, 114.2, 104.4, (C-H), 65.8, 61.7, 56.0 and 55.5 (CH_3). IR (KBr): 1678 cm^{-1} (Ar–C═O).

Reaction of CA1 Quinones Q1 and Q2 with Glutathione. Adding excess GSH to Q1 resulted in decoloration and formation of a polar, stable product (Figure 2) with a mass ~637.3 Da, consistent with the formation of a quinone–glutathione adduct $Q1H_2$-SG (Scheme 1) ($C_{28}H_{35}N_3O_{12}S$ = 637.19). GSH probably adds to the more electropositive of the positions potentially susceptible to Michael addition—likely to be that *ortho* to the vinylogous linker—although this has not been confirmed.

Q2 was prepared from CA1 by oxidation with $FeCl_3$ as described above, with 99% purity, and excess GSH was added. Chromatographic analysis showed loss of Q2 and formation of a major product over several minutes with retention character-

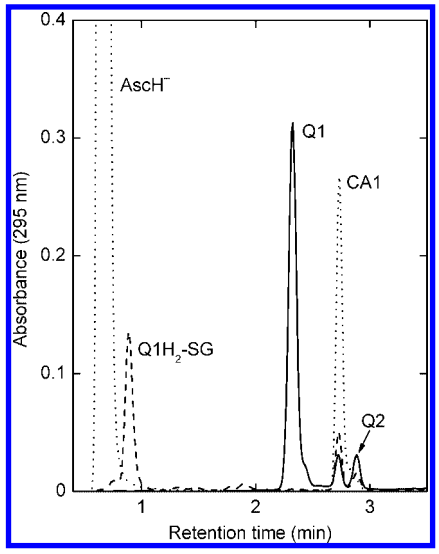

Figure 2. HPLC chromatograms showing Q1 and Q2 from oxidation of CA1 (2) by $FeCl_3/H_2SO_4$ (—); formation of CA1 from the reduction of Q1 with excess ascorbate (▪▪▪); and the product from the reaction of GSH with Q1, assigned to $Q1H_2$-SG (---) (see Scheme 1).

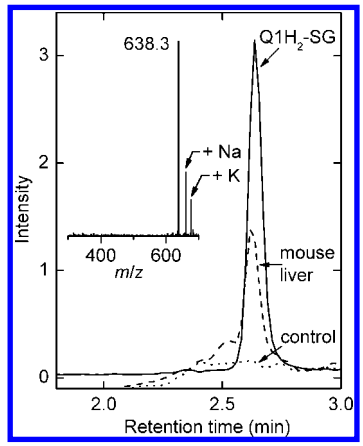

Figure 3. LC/MS chromatograms monitoring at $m/z = 638$, showing product prepared chemically by reaction of Q1 and GSH, assigned to $Q1H_2$-SG (—); chromatogram from mouse liver homogenate 18 min postadministration of CA1P (50 mg/kg) to a SCID mouse (---); and chromatogram from liver homogenate from a control SCID mouse (▪▪▪). Inset: mass spectrum from HPLC/MS; labeled masses correspond to protonated molecular ions.

istics similar to Q2 but slightly more polar, with λ_{max} 268 nm (Figure 1) and mass of ~330.2 Da, suggestive of reduction of Q2 to a hydroquinone $Q2H_2$ (Scheme 1). A minor product was observed, eluting earlier than $Q2H_2$ and with mass 635.4 corresponding to a GSH conjugate of Q2 (data not shown), but it was clear that GSH reduced Q2 in preference to addition, in contrast to Q1 where addition of GSH was the dominant reaction.

Tissue Distribution and Metabolism of CA1 after Administration to Mice. Free CA1 was found to be retained in mouse CaNT tumor tissue (9.2 μM) as compared to plasma (0.085 μM) and liver (2.0 μM) 2 h after IP injection of CA1P (50 mg/kg). A metabolite with HPLC retention characteristics and MS fragmentation patterns identical to that of $Q1H_2$-SG was observed in tumor, plasma, and liver tissues, with the highest levels found in the liver 15 min after dosing (Figure 3). The same product (mass ~637.3 Da) was measured in the liver of nontumor-bearing SCID mice after CA1 administration (Figure 3) and in ca. 100-fold lower amounts in plasma; no peak attributable to $Q1H_2$-SG was observed in kidney homogenates.

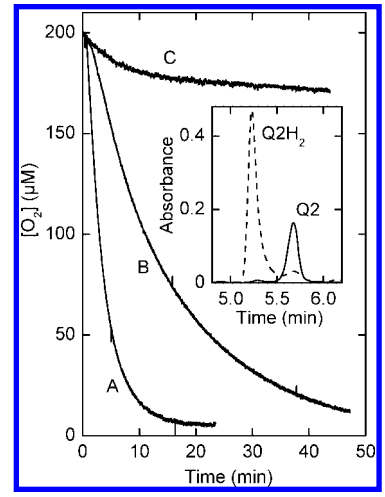

Figure 4. Depletion of oxygen in air-saturated solutions of Q2 (50 μM) in phosphate buffer (25 mM, pH 7.4) containing DTPA (100 μM) at 37 °C after the addition of (A) ascorbate (0.3 mM), (B) glutathione (3 mM), or (C) without addition. Insert: HPLC chromatograms at 268 nm showing Q2 (0.5 mM) (—) was reduced to QH_2 (---) by addition of ascorbate (5 mM).

Reactions of CA1 Quinones Q1 and Q2 with Ascorbate. The addition of excess ascorbate to Q1 showed immediate loss of Q1 with the reformation of CA1 (Figure 2). In Scheme 1, we have shown this to proceed via two one-electron steps, on the basis of EPR evidence for the ascorbate radical $Asc^{\bullet-}$ (see below). Reaction of Q2 with $AscH^-$ was shown to generate the same product as formed on reaction between Q2 and GSH, ascribed to the hydroquinone $Q2H_2$ (Scheme 1).

Oxygen Consumption during Reaction of CA1 Quinones with GSH or Ascorbate. Measurements using an oxygen electrode (Figure 4) showed that the oxygen concentration in air-saturated buffer containing Q2 at 37 °C was rapidly reduced on adding either ascorbate or GSH. Catalase (10 μg/mL) was not found to affect the rate of oxygen loss. HPLC analysis of the solutions after O_2 consumption was complete (Figure 4, insert) showed the formation of a product with the same UV spectrum (Figure 1) and mass (~330.1 Da) as seen in the previous LC/MS experiments and ascribed to $Q2H_2$.

Peroxidase-catalyzed oxidation of CA1 by HRP/H_2O_2 resulted in the formation of Q1, which decayed over a few minutes, leaving Q2 (Figure 5). There was slow oxygen consumption if ascorbate was added to a mixture of CA1 and HRP/H_2O_2 immediately on mixing CA1 with HRP/H_2O_2; however, if the addition of $AscH^-$ was delayed by a few minutes, thus facilitating build-up of Q2, O_2 was consumed more rapidly in a delay-time-dependent manner (Figure 5).

Production of Free Radicals during Oxidation of CA1 or CA4 and the Effects of GSH or Ascorbate. EPR signals were observed in aqueous solutions of CA1 at pH 7.4 (Figure 6). The signals were enhanced by adding $MgCl_2$, which stabilizes catechol semiquinone radicals (*16*). Figure 6A–C shows that similar signals were obtained from CA1 alone (autoxidation) or with added tyrosinase or HRP. Although in this experiment, signal B was ~40% lower in intensity than signal A, this simply reflects a shorter time standing in air in experiment B as compared to A. Autoxidation, possibly involving metal catalysis, was sufficient to produce a high "background" signal without added enzyme. The increase in signal intensity on adding either enzyme was never greater than 20% higher than without enzyme. Weak outer lines were evident in spectrum C, not seen in A. A similar signal (D) was observed on dissolving the oxidized product Q2 in $MgCl_2$ buffer. Analysis

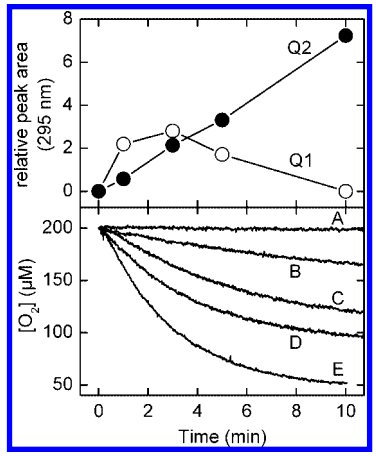

Figure 5. Top panel: HPLC peak areas of Q1 (○) and Q2 (●) after increasing times of reaction of CA1 (100 μM) with HRP (6.7 μg/mL) and H_2O_2 (10 μM), monitoring by HPLC at 295 nm; no ascorbate was present. Lower panel: depletion of oxygen in mixtures of CA1, HRP, and H_2O_2 as described above but with added ascorbate except for trace A. (A) CA1, HRP, and H_2O_2 alone; (B–E) CA1, H_2O_2, and HRP. Ascorbate (1 mM) was added either immediately after adding HRP (B) or 1 (C), 3 (D), or 10 min (E) after initiating reaction with HRP. Note that the traces in the lower panel all have the same zero time point, that is, the time that ascorbate was added.

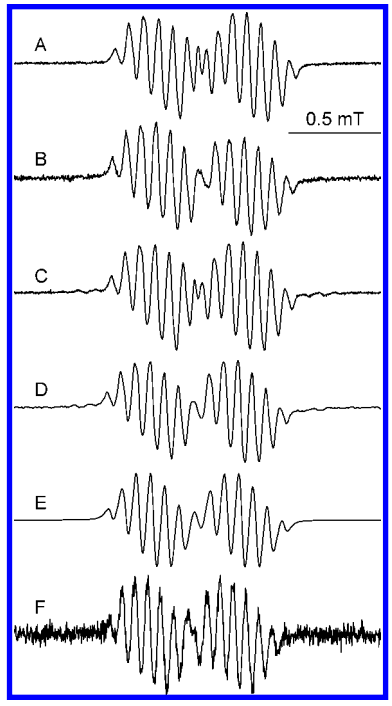

Figure 6. EPR spectra of radical(s) obtained from CA1 or Q2. (A–D) With 0.2 M $MgCl_2$: (A) CA1 (0.4 mM), Tris pH 7.4 (40 mM), 2% v/v DMSO; (B) same as A with 0.1 mg/mL tyrosinase; (C) same as A with 0.1 mg/mL HRP; and (D) 0.5 mM Q2 in phosphate buffer (0.2 M, pH 7.4), 10% v/v MeCN. (E) Simulated spectrum with $a_H = 0.481$ mT; $a_H = 0.153$, 0.081 (3), and 0.066 mT; line width, 0.027 mT; and 86% Lorentzian. (F) Without $MgCl_2$: CA1 (0.4 mM), Tris (40 mM, pH 7.4), tyrosinase (0.1 mg/mL), 37 °C, after 2 min.

of spectra A–D showed satisfactory simulations for three interacting protons together with the three protons of a methoxy substituent, with proton hyperfine splittings of $a_H = 0.479$–0.482, 0.150–0.155, 0.080–0.082 (three equivalent), and 0.061–0.075 mT; simulation E represents the mean values. Omitting $MgCl_2$ resulted in a ~four-fold weaker signal of overall similar pattern F but with mainly slightly reduced couplings: $a_H = 0.465$, 0.133, 0.068 (three equivalent), and 0.085 mT. Under similar conditions, no signals were observed from CA4.

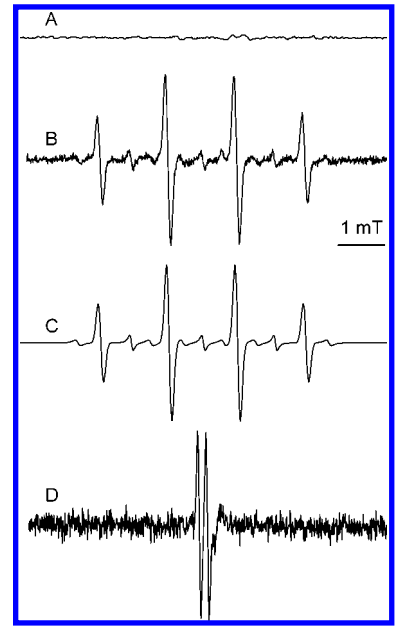

Figure 7. EPR spectra obtained from Q2 in the presence of DMPO (0.2 M), EtOH (10% v/v), DTPA (2 mM), and phosphate (0.2 M, pH 7.4): (A) GSH (5 mM), no Q2; (B) GSH (5 mM) and Q2 (50 μM) after 15 min; and (C) simulation of B with species 1 = 75% ($a_N = a_H = 1.49$ mT), species 2 = 15% ($a_N = 1.59$ mT and $a_H = 0.229$ mT), and species 3 = 10% ($a_N = 1.57$ mT). (D) ascorbate (5 mM) and Q2 (50 μM) after 15 min.

Because adding GSH or ascorbate to Q2 resulted in oxygen depletion (see above), we searched for intermediate radicals using the spin trap DMPO. Adding GSH to Q2 in the presence of DMPO gave the characteristic four-line signal from DMPO/$^{\bullet}$OH, plus weak contributions from other species (Figure 7B; no signal was seen without Q2 (trace A). Simulation (Figure 7C) showed a satisfactory fit assuming 75% of the signal came from DMPO/$^{\bullet}$OH (species 1), with 15% from a second species and 10% from a third, with the couplings indicated. On substituting GSH with ascorbate, these signals disappeared and only the doublet ($a_H = 0.179$ mT) of the ascorbate radical was observed. The latter radical is always present in solutions containing ascorbate, but its intensity was approximately trebled by the addition of Q2.

UV/vis Spectra of the Semiquinone Radicals from CA1 and Their Reactivity Toward Oxygen. Pulse radiolysis was used to characterize the spectra of the radicals obtained either on one-electron oxidation of CA1 ($Q1^{\bullet-}$, Figure 8A) or on one-electron reduction of Q2 ($Q2^{\bullet-}$, Figure 9A); Figure 8A also shows the spectrum of the radical obtained on oxidizing CA4 by $N_3^{\bullet}$. The absorbance change, and stability of the transient species, from oxidation of CA1 was similar in the absence and presence of oxygen (Figure 8B); oxidation of CA1 by the one-electron oxidant $N_3^{\bullet}$ occurred with a rate constant of 4.9×10^9 M^{-1} s^{-1} (data not shown). Figure 9A shows that both the powerful reductant, $CO_2^{\bullet-}$, and the much weaker reductant, $O_2^{\bullet-}$, reacted with Q2 to produce a transient radical with spectra that were closely similar. Reduction by $O_2^{\bullet-}$, unlike the case with $CO_2^{\bullet-}$, necessarily involves solutions containing O_2, but the transient radical produced was unreactive toward oxygen, at least over hundreds of microseconds (Figure 9B).

Comparison of Rates of Oxidation of CA1 and CA4 by Enzymes and Oxidation of CA1 in Cells. CA1 was found to be oxidized by HRP compound I, an oxidizing peroxidase intermediate (*19*), with the formation of HRP compound II. Second order rate constants of $7.7 \pm 0.2 \times 10^6$ (pH 7) or $9.0 \pm 0.2 \times 10^6$ M^{-1} s^{-1} (pH 7.4) were measured; similar

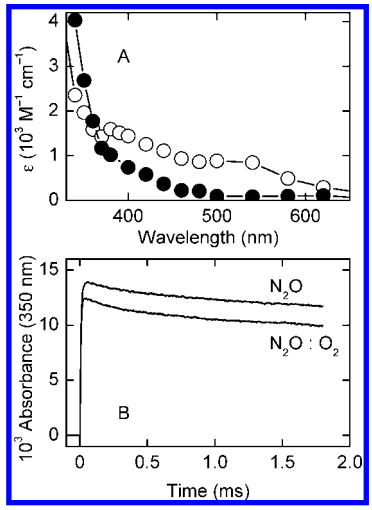

Figure 8. (A) Absorption spectra 50 μs after reaction of $N_3^\bullet$ with CA1 (●) or CA4 (○), obtained after pulse radiolysis (4.5 Gy) of N_2O-saturated solutions of the combretastatin (50 μM) with 0.1 M NaN_3, pH 7.4. (B) Absorbance/time traces showing the stability of the radical formed on oxidation of CA1 by $N_3^\bullet$ in solutions saturated with N_2O or N_2O:O_2 80:20 v/v.

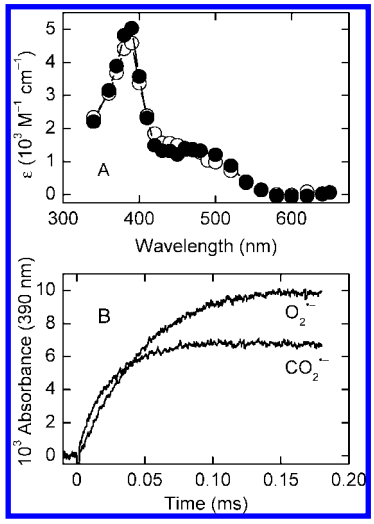

Figure 9. (A) Absorption spectra 200 μs after reaction of Q2 (30 μM) with either $CO_2^{\bullet-}$ (○) or $O_2^{\bullet-}$ (●), obtained on pulse radiolysis (3 Gy) of solutions containing $NaHCO_2$ (0.1 M), pH 7.4, saturated with O_2 or N_2O, respectively. (B) Absorbance/time traces at 390 nm under the same conditions.

experiments with HRP compound I and CA4 yielded rate constants of $3.4 \pm 0.2 \times 10^7$ (pH 7) or $5.1 \pm 0.1 \times 10^7$ M^{-1} s^{-1} (pH 7.4). Both lactoperoxidase and tyrosinase were also effective in oxidizing CA1 (100 μM) with 60–62 μM loss of CA1 in 80 min; similar experiments with CA4 and either enzyme resulted in 17–22 μM loss.

HL-60 (human promyelocytic leukemia) cells are rich in myeloperoxidase, but while CA1 (87 μM) was oxidized slowly by air at pH 7.4, 37 °C (7 μM lost in 60 min), this was not detectably accelerated on adding HL-60 cells ($\sim 2 \times 10^5$ cells/mL). However, adding SOD (125 μg/mL) markedly accelerated CA1 loss in the presence of HL60 cells (37 μM loss in 60 min). Q2 was identified in the extracellular medium.

Redox Properties of CA1, CA4, and Q2 Measured by Cyclic Voltammetry. Cyclic voltammetry experiments confirmed major differences in the redox properties of CA1 and CA4. While CA1 was oxidized at potentials <0.4 V vs NHE, the data suggest a mixture of two one-electron reversible reactions and a reduction potential for the CA1 radical ($QH^\bullet$/QH_2) of ~0.31 V vs NHE at pH 7.34 (Figure 10). CA4 was oxidized at much higher potentials, with a nonreversible wave at 0.85 V vs NHE. Cyclic voltammetry experiments with Q2 showed a two-electron, reversible reaction with a reduction potential of 0.16 V vs NHE.

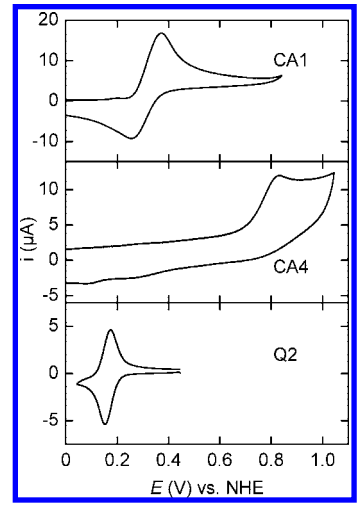

Figure 10. Cyclic voltammograms of CA1, CA4, or Q2 at pH 7.4.

Discussion

Combretastatin A-1 was found to be retained in murine tumors relative to plasma or liver as shown previously (*20*), presumably because of tumor vascular shut down trapping CA1 inside the tumor vessels. Oxidation of CA1 by Fe(III) formed two products, thought to be *ortho*-quinones Q1 and Q2 (Scheme 1); Q2 was fully characterized, while HPLC/MS provided support for the assignment to Q1. Further support for two different quinones was obtained by the different absorption spectra of radicals obtained on oxidation of CA1 (Figure 8A, assigned to $Q1^{\bullet-}$) or reduction of chemically synthesized Q2 (Figure 9A, assigned to $Q2^{\bullet-}$). While both Q1 and Q2 reacted with GSH, the former generated a thioether adduct $Q1H_2$-SG, while Q2 produced another catechol, $Q2H_2$, in preference to conjugating with GSH. Ascorbate served to reverse oxidation of both quinones, but $Q1H_2$-SG was detected in the liver, tumor, and plasma of mice administered with CA1P. High reactivities toward GSH and ascorbate of 4-methoxy-1,2-benzoquinone have been reported (*21*). The transformation of Q1 to $Q1H_2$-SG in vivo is likely to be catalyzed by glutathione-*S*-transferases [even fast conjugative reactions of GSH are catalyzed by this enzyme family (*22*)]. This study has thus revealed $Q1H_2$-SG as a possible marker for oxidative metabolism of CA1, via quinone formation and reaction with GSH. It is possible, like other GSH conjugates (*23*), that the thioether is degraded further to mercapturic acids; further work is needed to address this possibility.

In the absence of GSH, the quinone Q1 formed initially is transformed rapidly to a closed-ring quinone Q2; under no conditions was Q2 observed without prior formation of Q1. Figure 5 shows Q2 building up as Q1 decays after formation by enzyme-catalyzed oxidation of CA1. Electrocyclic ring closure of Q1 leaves only one carbon atom free to undergo Michael addition with GSH, whereas there are two possible sites in Q1. The methoxy group adjacent to the free carbon in Q2 will increase electronegativity at this site, rendering it less likely to be attacked by a nucleophile than the site suggested for GSH attack on Q1 in Scheme 1; there may also be less steric hindrance for attack by GSH in Q1 as compared to Q2. Thus,

ascorbate may be a potentially more important reductant than GSH for Q2, and the closed-ring hydroquinone $Q2H_2$ is an alternative, although possibly less abundant, marker of oxidative metabolism of CA1 than $Q1H_2$-SG. An earlier study (*20*) suggested formation of a quinone from CA1, with a mass fragment corresponding to Q2, but the product isolated from mouse plasma and suggested to be a quinone seems unlikely to be the same as either Q1 or Q2 in the present study: The HPLC conditions and retention times are consistent with a species more polar than a quinone, and the peak showed ions with masses as high as 451.2.

Peroxidases are obvious candidates for catalyzing oxidation of CA1 in vivo. The widely studied plant peroxidase, HRP, was shown to catalyze the formation of Q1, while CA1 was shown to be a substrate for the mammalian peroxidase, lactoperoxidase. Myeloperoxidase-rich HL-60 cells oxidized CA1, provided extracellular SOD was added. Macrophage infiltration of tumors may be a significant source of peroxidases. Phenols are good substrates for peroxidases, and higher reactivity of resorcinol (1,3-dihydroxybenzene) as compared to phenol for oxidation by HRP compound I is consistent with established redox relationships (*24, 25*). While the reactivity of both CA1 and CA4 toward HRP compound I is comparable to that for reaction of compound I with other phenols (*25*), the expected enhancement of reactivity accompanying the additional hydroxyl substituent in CA1 was not observed despite the much greater ease of oxidation of CA1 as compared to CA4 demonstrated by cyclic voltammetry. A speculative explanation for this behavior might be that oxidation of both combretastatins by HRP involves electron transfer from the trimethoxybenzene moiety to form a radical cation that deprotonates at phenolic oxygen to form phenoxyl radicals; evidence for oxidation of methoxybenzenes by HRP to produce radical cations has been presented (*26*).

Most peroxidases oxidize phenolic substrates via two one-electron steps (*19*), that is, producing phenoxyl radicals, or in the case of catechols, semiquinones. However, tyrosinase is thought to produce semiquinone radicals with catechols via "reverse disproportionation" or comproportionation (eq 1) (*27*), where QH_2 is the catechol and Q the corresponding quinone:

$$QH_2 + Q \rightleftarrows 2Q^{\bullet -} + 2H^+ \qquad (1)$$

Reductive addition of GSH to quinones, such as that forming the thioether hydroquinone $Q1H_2$-SG (Scheme 1), can also generate radicals via similar equilibria (*28, 29*). Partial aerobic oxidation of catechols, especially at alkaline pH, is sufficient to generate enough quinone such that semiquinones are readily observed in aqueous solutions, with EPR signals enhanced by complexing the semiquinones with Mg^{2+} or Zn^{2+} (*30*).

The EPR signals observed on oxidation of CA1 (Figure 6) might provide evidence for the semiquinones of Q1 and/or Q2, although a mixture of both could be formed, and the signal reflects the steady-state situation from multiple comproportionation equilibria of the form of eq 1. While small differences were apparent in the different experiments, the signal obtained from Q2 alone in the presence of Mg^{2+} (perhaps via reduction by metal ion contaminants) was similar to that obtained via CA1, suggesting at first sight that most of the signal observed during oxidation of CA1 arose from Q2 semiquinone.

In principle, the EPR spectra of the semiquinones of Q1 and Q2 should be readily distinguishable, since an interacting proton is lost in the latter on ring closure. In practice, the main features of the EPR spectra of $Q1^{\bullet -}$ and $Q2^{\bullet -}$ are probably rather similar. Thus, as pointers, we might compare $Q1^{\bullet -}$ with the semiquinone of 3-methoxycatechol and $Q2^{\bullet -}$ with that from 1,2-dihydronaphthoquinone. The dominant doublet splitting observed in this work, $a_H \sim 0.48$ mT (Figure 6), is similar to both the coupling to H-5 in 3-methoxycatechol (~0.48 mT) (*31, 32*) and the H-4 in 1,2-dihydroxynaphthalene semiquinone [~0.45 mT (*33*)]. [The semiquinone of Zn^{2+}-complexed 4-methoxycatechol shows the major proton hyperfine coupling only ~8% higher than that of the noncomplexed radical (*30*).] The observed methoxy proton coupling, ~0.081 mT (Figure 6), is similar to that in the semiquinone of 3-methoxycatechol [0.067 mT (*31, 32*)] but is likely to be comparable in both Q1 and Q2. The larger of the other two proton splittings that we extracted ($a_H \sim 0.15$ mT) is quite similar to the H-4 coupling in the semiquinone of 3-methoxycatechol [0.125 mT (*31, 32*)], but the semiquinone of 1,2-dihydroxynaphthalene has $a_H = 0.13$ mT for H-8 (*33*). The smallest and probably less well-defined coupling in the observed spectra (~0.07 mT) is closer to that of H-6 in 3-methoxycatechol semiquinone [~0.059 mT (*31, 32*)] than that of H-7 in the radical from 1,2-dihydroxynaphthalene [~0.014 mT (*33*)]. Likely proton couplings for the exocyclic, vinylogous protons in $Q1^{\bullet -}$ are difficult to estimate, but comparison can be made with the methyl protons in 3,4-dimethoxy-6-methylcatechol [$a_H = 0.185$ mT (*34*)] or the exocyclic proton couplings in caffeic acid (3,4-dihydroxycinnamic acid) [~0.24 and 0.12 mT (*35, 36*)]. Thus, $Q^{\bullet -}$ might well have a spectrum similar to that of the semiquinone of 3-methoxycatechol but with 1–2 additional proton couplings of ~0.2–0.1 mT; a contribution from $Q1^{\bullet -}$ might be responsible for the outer, weak lines additionally present in some spectra, for example, Figure 6C, but these were also present in the spectrum observed from Q2 (Figure 6D). Overall, it is difficult from the present work to assign the dominant signal unequivocally to $Q1^{\bullet -}$ or $Q2^{\bullet -}$, and further work is desirable using, for example, fast oxidation of CA1 in a flow system to observe the initial spectrum from the semiquinone before the formation of Q2 can occur.

Radical formation from reaction of Q2 with ascorbate or GSH was studied by EPR using DMPO as a spin trap. The signal seen with Q2 and GSH (Figure 7B) was predominantly the DMPO/$^{\bullet}$OH adduct (*37*), particularly strong after incubating at 37 °C for 15 min, but this is not evidence for production of a major component from free $^{\bullet}$OH radicals, since ethanol (10% v/v) was present. This would have scavenged $^{\bullet}$OH preferentially over DMPO, generating the $^{\bullet}CH(OH)CH_3$ radical, but only ~15% of the signal (Figure 7, species 2) was identifiable with the DMPO/$^{\bullet}CH(OH)CH_3$ adduct (*37*). The major component (DMPO/$^{\bullet}$OH) is instead thought to arise from reduction of the DMPO/$^{\bullet}$OOH (superoxide) adduct (*38*), possibly by GSH, superoxide, or the hydroquinone QH_2. The minor component (Figure 7, species 3) is assigned to an uncharacterized oxidation product of the spin trap that is sometimes seen in experiments involving strong oxidants (e.g., ref *39*). No DMPO-trapped radicals were observed in solutions containing Q2, ethanol, and ascorbate; this might be expected, since ascorbate reduces the ethanol radical–DMPO adducts to spin-silent products (*40*) and is much more reactive toward superoxide than DMPO. Instead, the characteristic signal of the ascorbate radical was enhanced by Q2.

There are two key features of the oxygen consumption experiments involving Q2 or CA1 and GSH or ascorbate (Figures 4 and 5). First, more oxygen is depleted than CA1 or Q2 added, showing that turnover of oxygen is a chain reaction. In another example of redox cycling, ~250 μM oxygen was consumed by lactoperoxidase/H_2O_2-catalyzed oxidation of 10

μM phenolphthalein (*41*). Second, oxygen consumption is greatly accelerated by the presence of Q2, either added initially (Figure 4) or allowed to form via Q1 on standing after reaction of CA1 with HRP/H_2O_2 (Figure 5). The latter figure shows the rate of oxygen consumption on adding ascorbate and was accelerated if the mixture of CA1 and HRP/H_2O_2 was allowed to stand for a few minutes to allow Q1 to decay to Q2.

Numerous studies have been made of redox cycling of oxygen catalyzed by quinones and GSH or ascorbate or hydroquinones, demonstrating complex reaction pathways involving both quinone and ascorbate free radical intermediates (*42–47*). A key equilibrium is electron transfer between semiquinone(s) and oxygen:

$$Q^{\bullet-} + O_2 \rightleftarrows Q + O_2^{\bullet-} \quad (2)$$

which, by comparison with other *ortho*-quinones, was expected to be over to the left for Q1 and Q2 ($K_2 < 1$) unless [O_2] >> [Q], since the midpoint electrode potentials E_m at pH ~7.4 of simple *ortho*-quinones are such that $E_m(Q/Q^{\bullet-}) > E_m(O_2[1\ M]/O_2^{\bullet-})$ (*48*). [The semiquinones are largely dissociated at pH 7.4 since the pK_a values of the conjugate acids of methoxy-substituted *ortho*-semiquinone radicals are ~5.0 (*32*).] The cyclic voltammetry behavior (Figure 10), the direct observation of rapid reaction of $O_2^{\bullet-}$ over tens of microseconds with only 30 μM Q2 and 1.25 mM O_2 (Figure 9B), and the lack of reactivity of $Q1^{\bullet-}$ with oxygen over milliseconds (Figure 8B) are all consistent with the expectation that eq 2 is indeed well over to the left with both Q1 and Q2. Studies with other *ortho*-semiquinones have reached similar conclusions (*49, 50*). Loss of CA1 in suspensions of HL60 cells was observed provided that SOD was added. This might be explained by SOD-catalyzed removal of $O_2^{\bullet-}$ driving eq 2 to the right, the semiquinone(s) being formed extracellularly from quinone(s) formed on intracellular oxidation of CA1 diffusing into the medium and generating semiquinone(s) via eq 1. The loss of CA1 in the presence of HL-60 cells could also be due, as a reviewer has suggested, to oxidation of CA1 by myeloperoxidase/H_2O_2 (especially in the presence of SOD, which catalyzes dismutation of superoxide to H_2O_2) and/or by a peroxidase-like activity of SOD itself.

Ascorbate reacts about as rapidly with $O_2^{\bullet-}$ as uncatalyzed dismutation of the latter radical (*51*), so that ascorbate enhances oxygen turnover in the presence of Q2, as observed (Figure 4). The EPR signal of the ascorbate radical was enhanced on adding Q2, reflecting the equilibrium:

$$Q + AscH^- \rightleftarrows Q^{\bullet-} + Asc^{\bullet-} (+ H^+) \quad (3)$$

which is an additional route to semiquinone radicals. A further complexity is reduction of semiquinone(s) to hydroquinone(s) by ascorbate:

$$Q^{\bullet-} + AscH^- (+ H^+) \rightleftarrows QH_2 + Asc^{\bullet-} \quad (4)$$

leading to a complex array of multiple equilibria, as discussed for simpler quinones by Roginsky et al. (*45–47*). Because of the instability of Q1, it is not possible to characterize fully corresponding pathways in the present study, although the results clearly point to the possibility of enhanced oxidative stress following oxidation of CA1 in vivo. Some evidence for reaction of $^{\bullet}OH$ with ethanol was observed in solutions containing Q2 and GSH (Figure 7). It is conceivable that this could involve in part hydroxyl radical formation, via reduction of H_2O_2 by semiquinones, formally

$$Q^{\bullet-} + H_2O_2 \rightarrow Q + {}^{\bullet}OH + OH^- \quad (5)$$

but likely to proceed via the involvement of metal ions rather than by direct reaction (*52–54*). The presence of chelators may not suppress such involvement (*55–57*), although desferrioxamine effectively inhibited the apparent reaction of adriamycin semiquinone with H_2O_2 (*53*).

Overall, the present study is consistent with the pathways summarized in Scheme 1. Oxidation of CA1 proceeds via a semiquinone radical to an *ortho*-quinone Q1, highly reactive toward ascorbate and superoxide, reforming the hydroquinone, CA1. Q1 is reactive toward thiols, thus raising the possibility, not investigated in this work, of binding to protein thiols in competition with reaction with GSH. These reactions are themselves in competition with the transformation of Q1 to Q2. The latter quinone catalyzes oxygen consumption and thus has the potential to enhance cellular oxidative stress. In contrast, combretastatin A-4, although shown to be oxidized by enzyme-catalyzed systems, does not stimulate oxygen turnover. The products of CA4 oxidation are likely to be dimers resulting from intermediate phenoxy radicals, similar to those arising from tyrosine oxidation (*58*).

In conclusion, the additional phenolic moiety in combretastatin A-1 as compared to A-4 markedly changes the redox properties of the molecules and introduces completely different chemical functionality. The *ortho*-quinones formed on oxidation of CA1 are key intermediates meriting further investigation. In particular, identification of adducts of other *ortho*-quinones not only with GSH but also with nucleotides (e.g., refs *59–61*) suggests that reactivity of oxidative metabolites of CA1 with both proteins and nucleic acids should be studied. Both alkylation and oxidative stress have been correlated with the diverse roles of quinones in toxicology, with several examples including *ortho*-quinone moieties (*62*).

Acknowledgment. This work was supported by Cancer Research UK Programme Grants (C134/A2001 and A7428) and Oxigene Inc. We thank Dr. M. J. Burkitt for EPR experiments demonstrating the formation of radicals in crude oxidation mixtures of CA1, before we understood the two-step process and separated the two quinones; Dr. R. P. Mason for the supply of purified DMPO and helpful discussions; and K. B. Patel for help with pulse radiolysis experiments.

Supporting Information Available: ^1H and ^{13}C NMR and MS spectra of Q2. This material is available free of charge via the Internet at http://pubs.acs.org.

References

(1) Thorpe, P. E., Chaplin, D. J., and Blakey, D. C. (2003) The first international conference on vascular targeting agents: Meeting overview. *Cancer Res. 2003*, 1144–1147.

(2) Siemann, D. W., Chaplin, D. J., and Horsman, M. R. (2004) Vascular-targeting therapies for treatment of malignant disease. *Cancer 100*, 2491–2499.

(3) Neri, D., and Bicknell, R. (2005) Tumour vascular targeting. *Nat. Rev. Cancer 5*, 436–446.

(4) Horsman, M. R., and Siemann, D. W. (2006) Pathophysiologic effects of vascular-targeting agents and the implications for combination with conventional therapies. *Cancer Res. 66*, 11520–11539.

(5) Lin, C. M., Singh, S. B., Chu, P. S., Dempcy, R. O., Schmidt, J. M., Pettit, G. R., and E, H. (1988) Interactions of tubulin with potent natural and synthetic analogs of the antimitotic agent combretastatin: A structure-activity study. *Mol. Pharmacol. 34*, 200–208.

(6) Tozer, G. M., Kanthou, C., Parkins, C. S., and Hill, S. A. (2002) The biology of the combretastatins as tumour vascular targeting agents. *Int. J. Exp. Pathol. 83*, 21–38.

(7) Cooney, M. M., Ortiz, J., Bukowski, R. M., and Remick, S. C. (2005) Novel vascular targeting/disrupting agents: Combretastatin A4 phosphate and related compounds. *Curr. Oncol. Rep. 7*, 90–95.
(8) Chaplin, D. J., Horsman, M. R., and Siemann, D. W. (2006) Current development status of small-molecule vascular disrupting agents. *Curr. Opin. Invest. Drugs 7*, 522–528.
(9) Dowlati, A., Robertson, K., Cooney, M., Petros, W. P., Stratford, M., Jesberger, J., Rafie, N., Overmoyer, B., Makkar, V., Stambler, B., Taylor, A., Waas, J., Lewin, J. S., McCrae, K. R., and Remick, S. C. (2002) A phase I pharmacokinetic and translational study of the novel vascular targeting agent combretastatin A-4 phosphate on a single-dose intravenous schedule in patients with advanced cancer. *Cancer Res. 62*, 3408–3416.
(10) Rustin, G. J. S., Galbraith, S. M., Anderson, H., Stratford, M., Folkes, L. K., Sena, L., Gumbrell, L., and Price, P. (2003) Phase I clinical trial of weekly combretastatin A4 phosphate: Clinical and pharmacokinetic results. *J. Clin. Oncol. 21*, 2815–2822.
(11) Gaya, A. M., and Rustin, G. J. S. (2005) Vascular disrupting agents: a new class of drug in cancer therapy. *Clin. Oncol. (R. Coll. Radiol.) 17*, 277–290.
(12) Hill, S. A., Tozer, G. M., Pettit, G. R., and Chaplin, D. J. (2002) Preclinical evaluation of the antitumour activity of the novel vascular targeting agent Oxi 4503. *Anticancer Res. 22*, 1453–1458.
(13) Holwell, S. E., Thompson, M. J., Pettit, G. R., Lippert, L. W., III, Martin, S. W., and Bibby, M. C. (2002) Anti-tumor and anti-vascular effects of the novel tubulin-binding agent combretastatin A-1 phosphate. *Anticancer Res. 22*, 3933–3940.
(14) Hua, J., Sheng, Y., Pinney, K. G., Garner, C. M., Kane, R. R., Prezioso, J. A., Pettit, G. R., Chaplin, D. J., and Edvardsen, K. (2003) Oxi4503, a novel vascular targeting agent: Effects on blood flow and antitumor activity in comparison to combretastatin A-4 phosphate. *Anticancer Res. 23*, 1433–1440.
(15) McGown, A. T., and Fox, B. W. (1990) Differential cytotoxicity of combretastatins A1 and A4 in to daunorubicin-resistant P388 cell lines. *Cancer Chemother. Pharmacol. 26*, 79–81.
(16) Kalyanaraman, B., Premovic, P. I., and Sealy, R. C. (1987) Semiquinone anion radicals from addition of amino acids, peptides, and proteins to quinones derived from oxidation of catechols and catecholamines. An ESR spin stabilization study. *J. Biol. Chem. 262*, 11080–11087.
(17) Candeias, L. P., Folkes, L. K., Porssa, M., Parrick, J., and Wardman, P. (1996) Rates of reaction of indoleacetic acids with horseradish peroxidase compound I and their dependence on the redox potentials. *Biochemistry 35*, 102–108.
(18) Candeias, L. P., Folkes, L. K., Dennis, M. F., Patel, K. B., Everett, S. A., Stratford, M. R. L., and Wardman, P. (1994) Free-radical intermediates and stable products in the oxidation of indole-3-acetic acid. *J. Phys. Chem. 98*, 10131–10137.
(19) Dunford, H. B. (1999) *Heme Peroxidases*, Wiley-VCH, New York.
(20) Kirwan, I. G., Loadman, P. M., Swain, D. J., Anthoney, A. A., Pettit, G. R., Lippert, J. W., III, Shnyder, S. D., Cooper, P. A., and Bibby, M. C. (2004) Comparative preclinical pharmacokinetic and metabolic studies of the combretastatin prodrugs combretastatin A4 phosphate and A1 phosphate. *Clin. Cancer Res. 10*, 1446–1453.
(21) Land, E. J., Cooksey, C. J., and Riley, P. A. (1990) Reaction kinetics of 4-methoxy ortho benzoquinone in relation to its mechanism of cytotoxicity: A pulse radiolysis study. *Biochem. Pharmacol. 39*, 1133–1135.
(22) Coles, B., Wilson, I., Wardman, P., Hinson, J. A., Nelson, S. D., and Ketterer, B. (1988) The spontaneous and enzymic reaction of N-acetyl-p-benzoquinonimine with glutathione: A stopped-flow kinetic study. *Arch. Biochem. Biophys. 264*, 253–280.
(23) Sies, H., and Ketterer, B., Eds. (1988) *Glutathione Conjugation. Mechanisms and Biological Significance*, Academic Press, London.
(24) Job, D., and Dunford, H. B. (1976) Substituent effect on the oxidation of phenols and aromatic amines by horseradish peroxidase compound I. *Eur. J. Biochem. 66*, 607–614.
(25) Candeias, L. P., Folkes, L. K., and Wardman, P. (1997) Factors controlling the substrate specificity of peroxidases: Kinetic and thermodynamics of the reaction of horseradish peroxidase compound I with phenols and indole-3-acetic acids. *Biochemistry 36*, 7081–7085.
(26) Kersten, P. J., Kalyanaraman, B., Hammel, K. E., Reinhammar, B., and Kirk, T. K. (1990) Comparison of lignin peroxidase, horseradish peroxidase and laccase in the oxidation of methoxybenzenes. *Biochem. J. 268*, 475–480.
(27) Mason, H. S., Spencer, E., and Yamazaki, I. (1961) Indentification by electron spin resonance spectroscopy of the primary product of tyrosinase-catlayzed catechol oxidation. *Biochem. Biophys. Res. Commun. 4*, 236–238.
(28) Gant, T. W., D'Arcy Doherty, M., Odowole, D., Sales, K. D., and Cohen, G. M. (1986) Semiquinone anion radicals formed by the reaction of quinones with glutathione or amino acids. *FEBS Lett. 201*, 296–300.
(29) Takahashi, N., Schreiber, J., Fischer, V., and Mason, R. P. (1987) Formation of glutathione-conjugated semiquinones by the reaction of quinones with glutathione: An ESR study. *Arch. Biochem. Biophys. 252*, 41–48.
(30) Kalyanaraman, B., Felix, C. C., and Sealy, R. C. (1985) Semiquinone anion radicals of catechol(amine)s, catechol estrogens, and their metal ion complexes. *Environ. Health Perspect. 64*, 185–198.
(31) Holton, D. M., and Murphy, D. (1982) Solvent effects in the electron spin resonance spectra of semiquinones. *J. Chem. Soc., Faraday Trans. I 78*, 1223–1236.
(32) Steenken, S., and O'Neill, P. (1977) Oxidative demethoxylation of methoxylated phenols and hydroxybenzoic acids by the OH radical. An in situ electron spin resonance, conductimetric pulse radiolysis, and product analysis study. *J. Phys. Chem. 81*, 505–508.
(33) Ashworth, P., and Dixon, W. T. (1974) An electron spin resonance study of the autoxidation of naphthols in the presence of hydrogen peroxide. *J. Chem. Soc., Perkin Trans. 2*, 739–744.
(34) Holton, D. M., and Murphy, D. (1980) The electron spin resonance spectra of semiquinones obtained from some naturally occurring methoxybenzoquinones. *J. Chem. Soc., Perkin Trans. 2*, 1757–1759.
(35) Ashworth, P. (1976) Electron spin resonance studies of structure and conformation in anion radicals formed during the autoxidation of hydroxylated coumarins. *J. Org. Chem. 41*, 2920–2924.
(36) Bors, W., Michel, C., Stettmaier, K., Lu, Y., and Foo, L. P. (2003) Pulse radiolysis, electron paramagnetic resonance spectroscopy and theoretical calculations of caffeic acid oligomer radicals. *Biochim. Biophys. Acta 1620*, 97–107.
(37) Li, A. S. W., Cummings, K. B., Roethling, H. P., Buettner, G. R., and Chignell, C. F. (1988) A spin trapping database implemented on the IBM PC/AT. J. Magn. Reson. *79*, 140–142; http://epr.niehs.nih.gov/stdb.html.
(38) Buettner, G. R. (1993) The spin trapping of superoxide and hydroxyl free radicals with DMPO (5,5-dimethylpyrroline-N-oxide): More about iron. *Free Radical Res. Commun. 19* (Suppl.), S79–S87.
(39) Reszka, K. J., and Chignell, C. F. (1995) One-electron reduction of arenediazonium compounds by physiological electron donors generates aryl radicals. An EPR and spin trapping investigation. *Chem.-Biol. Interact. 96*, 223–234.
(40) Stoyanovsky, D. A., Wu, D., and Cederbaum, A. L. (1998) Interaction of 1-hydroxyethyl radical with glutathione, ascorbic acid and α-tocopherol. *Free Radical Biol. Med. 24*, 132–138.
(41) Sipe, H. J., Jr., Jordan, S. J., Hanna, P. M., and Mason, R. P. (1994) The metabolism of 17β-estradiol by lactoperoxidase: A possible source of oxidative stress in cancer. *Carcinogenesis 15*, 2637–2643.
(42) Brunmark, A., and Cadenas, E. (1989) Redox and addition chemistry of quinoid compounds and its biological implications. *Free Radical Biol. Med. 7*, 435–477.
(43) Goin, J., Gibson, D. D., McCay, P. B., and Cadenas, E. (1991) Glutathionyl- and hydroxyl radical formation coupled to the redox transitions of 1,4-naphthoquinone bioreductive alkylating agents during glutathione two-electron reductive addition. *Arch. Biochem. Biophys. 288*, 386–396.
(44) O'Brien, P. J. (1991) Molecular mechanisms of quinone cytotoxicity. *Chem.-Biol. Interact. 80*, 1–41.
(45) Roginsky, V. A., Barsukova, T. K., Bruchelt, G., and Stegmann, H. B. (1998) Kinetics of redox interaction between substituted 1,4-benzoquinones and ascorbate under aerobic conditions: Critical phenomena. *Free Radical Res. 29*, 115–125.
(46) Roginsky, V. A., Barsukova, T. K., and Stegmann, H. B. (1999) Kinetics of redox interaction between substututed quinones and ascorbate under aerobic conditions. *Chem.-Biol. Interact. 121*, 177–197.
(47) Roginsky, V., and Barsukova, T. (2000) Kinetics of oxidation of hydroquinones by molecular oxygen. Effect of superoxide dismutase. *J. Chem. Soc., Perkin Trans. 2*, 1575–1582.
(48) Wardman, P. (1989) Reduction potentials of one-electron couples involving free radicals in aqueous solution. *J. Phys. Chem. Ref. Data 18*, 1637–1755.
(49) Cooksey, C. J., Land, E. J., Riley, P. A., Sarna, T., and Truscott, T. G. (1987) On the interaction of anisyl-3,4-semiquinone with oxygen. *Free Radical Res. Commun. 4*, 131–138.
(50) Kalyanaraman, B., Korytowski, W., Pilas, B., Sarna, T., Land, E. J., and Truscott, T. G. (1988) Reaction between *ortho*-semiquinones and oxygen: pulse radiolysis, electron spin resonance, and oxygen uptake studies. *Arch. Biochem. Biophys. 266*, 277–284.
(51) Bielski, B. H. J., Cabelli, D. E., and Arudi, R. L. (1985) Reactivity of HO_2/O_2^- radicals in aqueous solution. *J. Phys. Chem. Ref. Data 14*, 1041–1100.
(52) Sushkov, D. G., Gritsan, N. P., and Weiner, L. M. (1987) Generation of OH radical during enzymatic reduction of 9,10-anthraquinone-2-sulphonate. Can semiquinone decompose hydrogen peroxide? *FEBS Lett. 225*, 139–144.

(53) Kalyanaraman, B., Morehouse, K. M., and Mason, R. P. (1991) An electron paramagnetic resonance study of the interactions between the adriamycin semiquinone, hydrogen peroxide, iron-chelators, and radical scavengers. *Arch. Biochem. Biophys. 286*, 164–170.

(54) Li, B., Gutierrez, P. L., Amstad, P., and Blough, N. V. (1999) Hydroxyl radical production by mouse epidermal cell lines in the presence of quinone anti-cancer compounds. *Chem. Res. Toxicol. 12*, 1042–1049.

(55) Morehouse, K. M., and Mason, R. P. (1988) The transition metal-mediated formation of the hydroxyl free radical during the reduction of molecular oxygen by ferredoxin-ferredoxin:$NADP^+$ oxidoreductase. *J. Biol. Chem. 263*, 1204–1211.

(56) Buettner, G. R., and Mason, R. P. (1990) Spin-trapping methods for detecting superoxide and hydroxyl free radicals *in vitro* and *in vivo*. *Methods Enzymol. 186*, 127–133.

(57) Burkitt, M. J. (1993) ESR spin trapping studies into the nature of the oxidizing species formed in the Fenton reaction: Pitfalls associated with the use of 5,5-dimethyl-1-pyrroline-N-oxide in the detection of the hydroxyl radical. *Free Radical Res. Commun. 18*, 43–57.

(58) Jin, F., Leitich, J., and von Sonntag, C. (1993) The superoxide radical reacts with tyrosine-derived phenoxyl radicals by addition rather than by electron transfer. *J. Chem. Soc., Perkin Trans. 2*, 1583–1588.

(59) Qiu, S.-X., Yang, R. Z., and Gross, M. L. (2004) Synthesis and liquid chromatography/tandem mass spectrometric characterization of the adducts of bisphenol A *o*-quinone with glutathione and nucleotide monophosphates. *Chem. Res. Toxicol. 17*, 1038–1046.

(60) Fan, Y., Schreiber, E. M., Giorgianni, A., Yalowich, J. C., and Day, B. W. (2006) Myeloperoxidase-catalyzed metabolism of etoposide to its quinone and glutathione adduct forms in HL60 cells. *Chem. Res. Toxicol. 19*, 937–943.

(61) Li, G., Zhang, H., Sader, F., Vadhavkar, N., and Njus, D. (2007) Oxidation of 4-methylcatechol: Implications for the oxidation of catecholamines. *Biochemistry 46*, 6978–6983.

(62) Bolton, J. L., Trush, M. A., Penning, T. M., Dryhurst, G., and Monks, T. J. (2000) Role of quinones in toxicology. *Chem. Res. Toxicol. 13*, 135–160.

TX7002195